Least–Squares Self–Calibration of Imaging Array Data

R. G. Arendt[1,2,3], S. H. Moseley[1], D. J. Fixsen[1,2]

[1] *Code 685, NASA/GSFC, Greenbelt, MD, 20771*
[2] *Science Systems & Applications, Inc.*
[3] *arendt@stars.gsfc.nasa.gov*

ABSTRACT

When arrays are used to collect multiple appropriately–dithered images of the same region of sky, the resulting data set can be calibrated using a least–squares minimization procedure that determines the optimal fit between the data and a model of that data. The model parameters include the desired sky intensities as well as instrument parameters such as pixel–to–pixel gains and offsets. The least–squares solution simultaneously provides the formal error estimates for the model parameters. With a suitable observing strategy, the need for separate calibration observations is reduced or eliminated.

We show examples of this calibration technique applied to HST NICMOS observations of the Hubble Deep Fields and simulated SIRTF IRAC observations.

1. Overview

Dithered images of the sky can contain sufficient information to determine both the sky intensities and the instrument properties without the use of separate calibration data. The best set of parameters describing the sky and the instrument can be obtained through a least–squares solution of the over–determined system of linear equations that model the data.

In this process, each point on the sky serves as a stable calibration source which is used to set the relative calibration of a subset of the detector pixels. The overlap between subsets for various points on the sky establishes the relative calibration of all detector pixels.

A much more complete description of the least–squares calibration can be found in Fixsen, Moseley, & Arendt (2000) and Arendt, Fixsen, & Moseley (2000). The notation used here follows that used in these references.

2. Data Models

The current version of the code calculates least–squares calibrations for data D^i that are described by any of the following three models:

$$D^i = S^\alpha G^p \quad (1)$$

$$D^i = S^\alpha G^p + F^p \quad (2)$$

$$D^i = S^\alpha G^p + F^p + F^q \quad (3)$$

where S^α is the sky intensity at position α, G^p is the detector gain at pixel p, F^p is the detector offset at pixel p, and F^q is a detector offset that can vary from frame to frame but

is constant over a) a whole frame, b) each quadrant of a frame (e.g. *HST* NICMOS), or c) alternating columns of a frame (e.g. *SIRTF* IRAC).

3. Algorithm Description

Our algorithm is a least–squares fit. As such, the solution for both the sky and detector parameters, X, can be computed as

$$X = (HWH)^{-1}HWD \tag{4}$$

where D is the data, W is the weight or inverse of the covariance matrix, and H is the mapping from the data to the detector pixels and sky positions (i.e the data model). Our algorithm takes advantage of the facts that 1) W is diagonal, 2) H is sparse and maps each datum to a single sky position, and 3) known singularities can be treated. The matrix HWH is divided into detector (A) and sky (C) portions as

$$HWH = \begin{pmatrix} A & B \\ B^T & C \end{pmatrix} \tag{5}$$

The mapping within H means that C is diagonal. Hence we express the portion of the inverse matrix related to the detector parameters as

$$(HWH)^{-1} = (A - BC^{-1}B^T)^{-1} = A^{-1/2}(I - TT^T)^{-1}A^{-1/2} = A^{-1/2}\left[\sum (TT^T)^n\right]A^{-1/2} \tag{6}$$

where $T \equiv A^{-1/2}BC^{-1/2}$ and T retains the sparse features of H.

4. Code Description

Direct evaluation of $(HWH)^{-1}$ would require inverting a $P \times P$ matrix where P is the number of parameters in the model. For a modest 256×256 array and a model including gains and offsets, $P > 2 \times 10^5$. By instead using the series expansion and making use of the sparse structure of H, our code avoids the direct inversion of such large matrices and never needs to handle arrays larger than twice the size of the data set which is being calibrated. Calculation of formal statistical uncertainties are a minor variation of the calculation of the solution itself. The code is written in IDL, with some calls to simple C functions. For efficiency in speed and memory, the structure of the code is related to the types of parameters in the data model.

5. Benefits and Features

A short list of some of the advantages of using a self–calibration procedure are:
1) Data can be calibrated without time lost to dedicated calibration observations.
2) Since the science data determine the calibration, the calibration is perfectly matched to the time and conditions of the science data collection.
3) The data model (H) clearly specifies any assumptions, avoiding hidden assumptions of ad hoc calibration plans.
4) Calibration can be derived in cases with few dithers if several fields are observed and

instrument parameters are stable or modeled.

6. Dithering Issues

A good dither pattern establishes direct calibrations for many pairs of pixels on all spatial scales regardless of the calibration method to be used. Any desired subpixel dithering may be superimposed on the main pattern. Subpixel dithering may be desirable for improving the resolution of data collected with detectors that undersample the instrument PSF. Figure 1 shows examples of one bad and two good dither patterns.

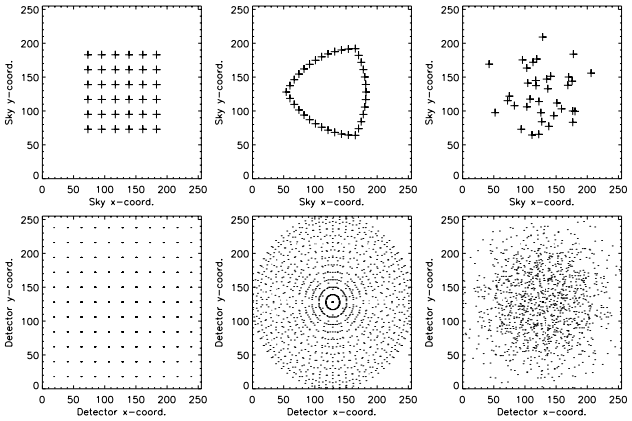

Fig. 1.— The top row shows three examples of 36–position dither patterns. The bottom row shows the corresponding patterns of all detector pixels that can be directly calibrated against the center pixel (for this example) of the array, by virtue of having observed a common position on the sky. The grid pattern at left is bad because it only provides calibrations between detector pixels at fixed intervals. The Reuleaux triangle and random patterns are good at providing calibrations on a wide range of scales.

7. Examples

The least–squares calibration code has been tested using *HST* NICMOS data for the HDF–N and HDF–S. These data were calibrated using the data model given by eq. (3), in which the F^q term contains the derived corrections for the "pedestal" effect that afflicts NICMOS data. The procedure contains no requirements on the spatial locations of the data being calibrated, only that the sky and detector parameters are fixed over the time of the observations. Therefore, we have processed HDF–N and HDF–S data as a single data set. This allows the HDF–N data which was collected with a relatively poor grid–like dither pattern to benefit from the more favorable dithering that was used for the HDF–S. Figures 2 and 3 show the resulting calibrated images for data taken with the F110W and F160W filters. For the HDF–N F160W observations, some of the HDF–N observations exhibit a different sky background level than the main field. Since these data would invalidate the assumption that the sky intensities S^α are constant, we processed these data as if the were at a third location (leftmost field in Fig. 3). In effect, the sky index α can be used to indicate both position and epoch of the observations in cases where the sky intensity varies.

Examination of the calibration of individual frames from the F110W data shows that

some frames are better calibrated than others (Fig. 4). The poorly calibrated frames turn out to be those observation for which the angle between the HDF and earth limb was smallest, and which appear to have elevated sky background levels. The results in Figure 4 show how the calibration of some of the data may be affected in cases where variable sky intensities are present, but ignored.

8. Dark Frames

Including dark frames as part of the data set to be calibrated can help prevent degeneracy between detector gain and offset parameters for low contrast targets. In this degeneracy a term x^p, which is fixed over time but may vary across the detector, may be subtracted from the gain and added to the offset after scaling by the mean sky intensity, without significantly changing the fit to the data:

$$D^i = G^p S^a + F^p \approx (G^p - x^p)S^\alpha + (F^p + x^p \langle S^\alpha \rangle) \tag{7}$$

If dark frames are unavailable, the degeneracy can be broken by observing a sky field or fields with significant contrast, such that $S^\alpha \neq \langle S^\alpha \rangle$, as in the examples below. Also, dark frames provide an absolute zero point reference for the sky and detector which can only be recovered from the sky observations with additional assumptions. About 1% of the HDF data in the previous examples were dark frames.

REFERENCES

Fixsen, D. J., Moseley, S. H., & Arendt, R. G. 2000, ApJS, 128, 651

Arendt, R. G., Fixsen, D. J., & Moseley, S. H. 2000, ApJ, 536, 500

Arendt, R. G., Fixsen, D. J., & Moseley, S. H. 2001, ADASS XI Conference Procedings, in press. (A long form of this is also available at http://cfa-www.harvard.edu/cfa/oir/Research/irac/arendt_hdf_preprint.pdf)

This work is support by the *SIRTF* IRAC instrument team. We thank M. Ashby for building the IRAC Science Data Simulator, and J. Surace for preparing the simulated data sets.

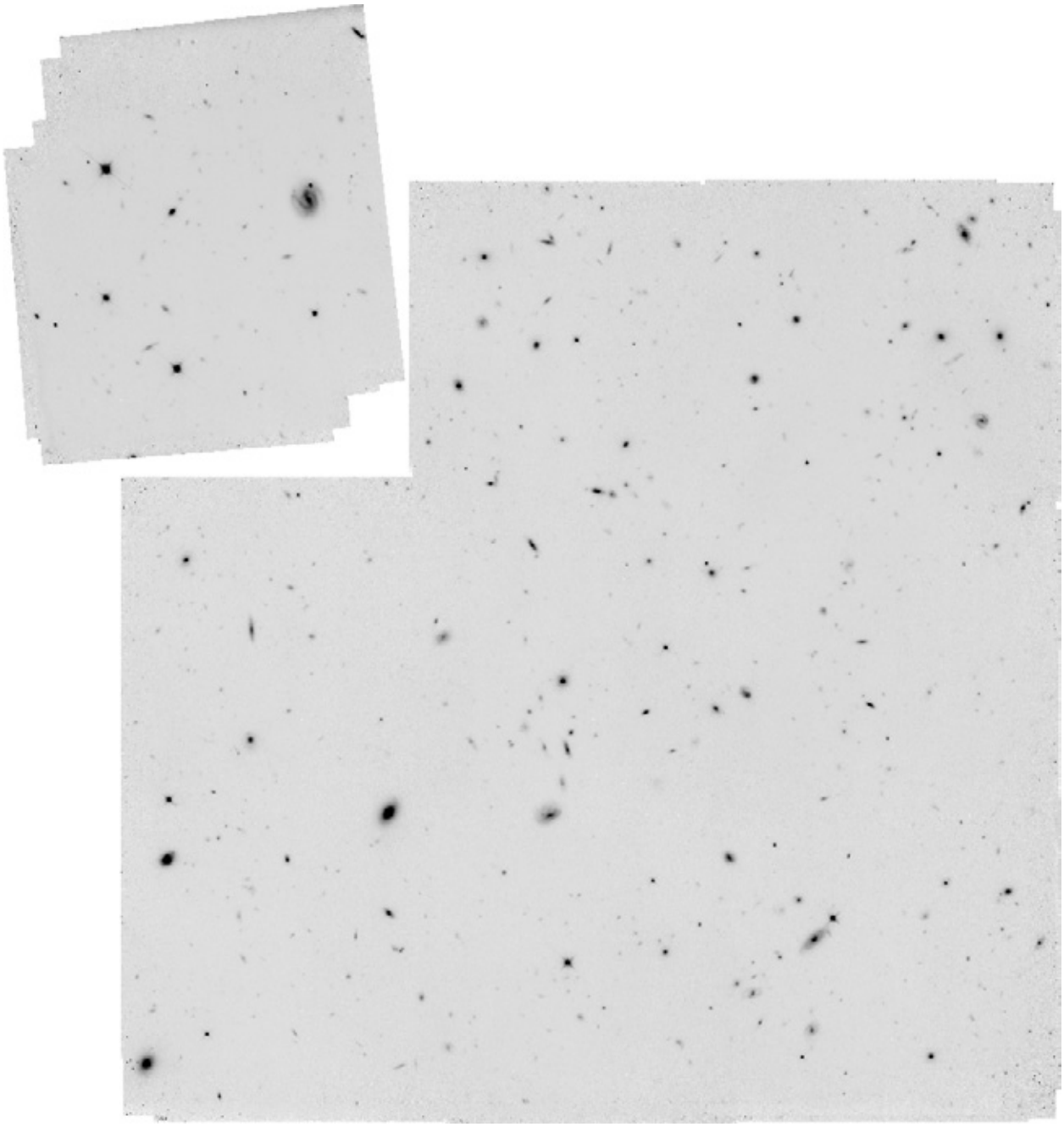

Fig. 2.— The least–squares self–calibrated image of the HDF–N (large area) and HDF–S (small area) in the NICMOS F110W filter. Displayed with square root intensity scaling.

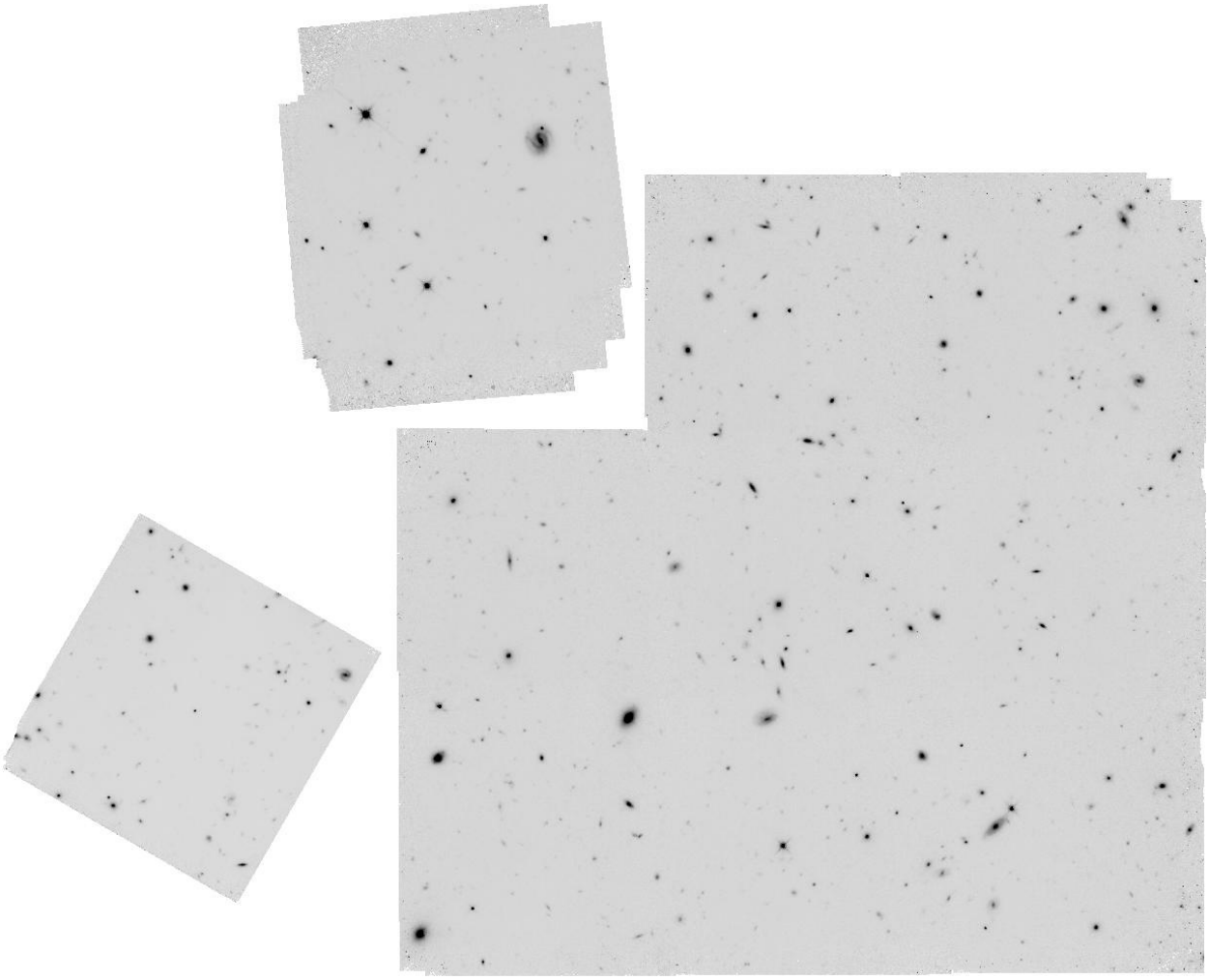

Fig. 3.— The least–squares self–calibrated image of the HDF–N (large area) and HDF–S (small area, upper left.) in the NICMOS F160W filter. The small region at left, is a portion of the HDF–N field that was observed at a different epoch and with a different background level, and was thus processed as if it was a third sky location. Displayed with square root intensity scaling.

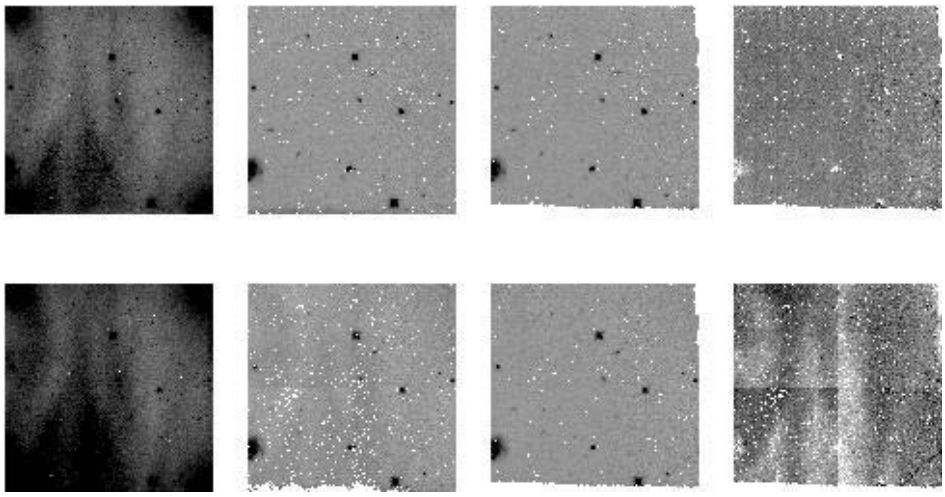

Fig. 4.— Left to right are: a single raw NICMOS frame, the same frame with calibrated via the least–squares self–calibration, the same frame as calibrated by processing at STSCI, and the difference between the two calibrated frames. The top row shows a frame for which the self–calibration solution works well. The second row shows a frame which had different sky background level than most of the data, and is consequently poorly calibrated by the same solution.

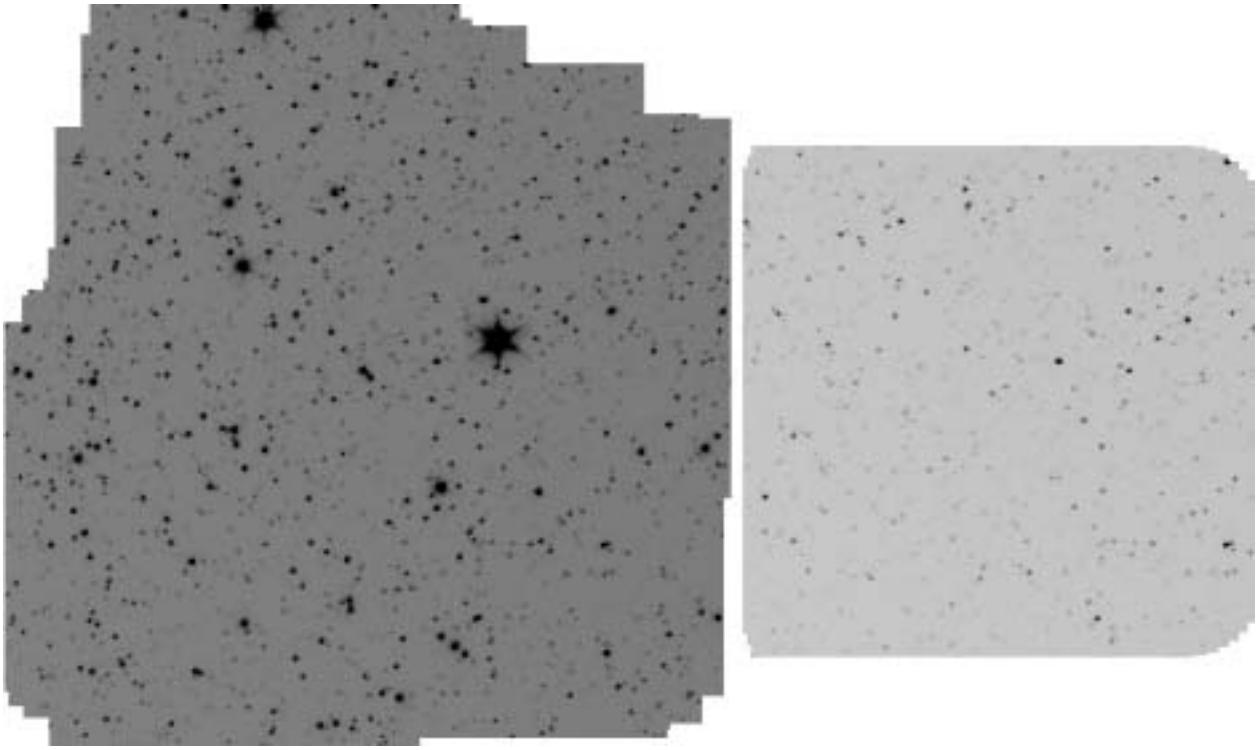

Fig. 5.— An example of simulateously processing fields with two different sky levels, to avoid degeneracies in the self–calibration solution without the use of dark frames. These are simulated IRAC data at low and high ecliptic latitudes.

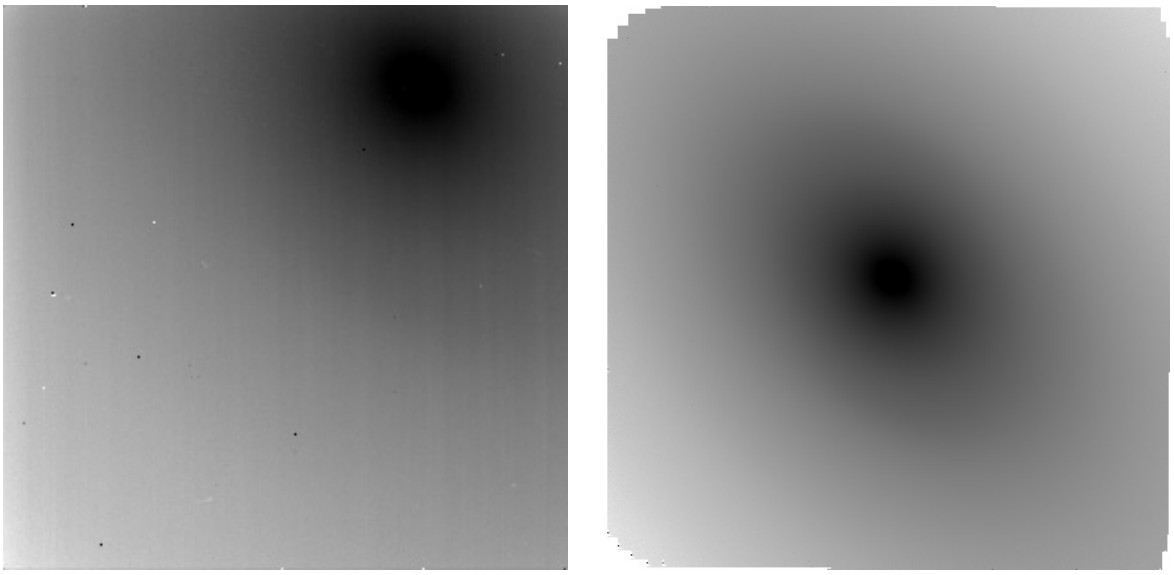

Fig. 6.— An example of using a single field with high contrast to avoid degeneracies in the self–calibration solution without the use of dark frames. This field is simulated IRAC observations of a model of the M 31 surface brightness. On the left is a single raw frame. Detector gain variations are small compared to the sky intensity variation, and may be hard to see in this reproduction. On the right is the calibrated final image. The full image is reduced in scale by a factor of ~ 2 compared to the single frame at left.

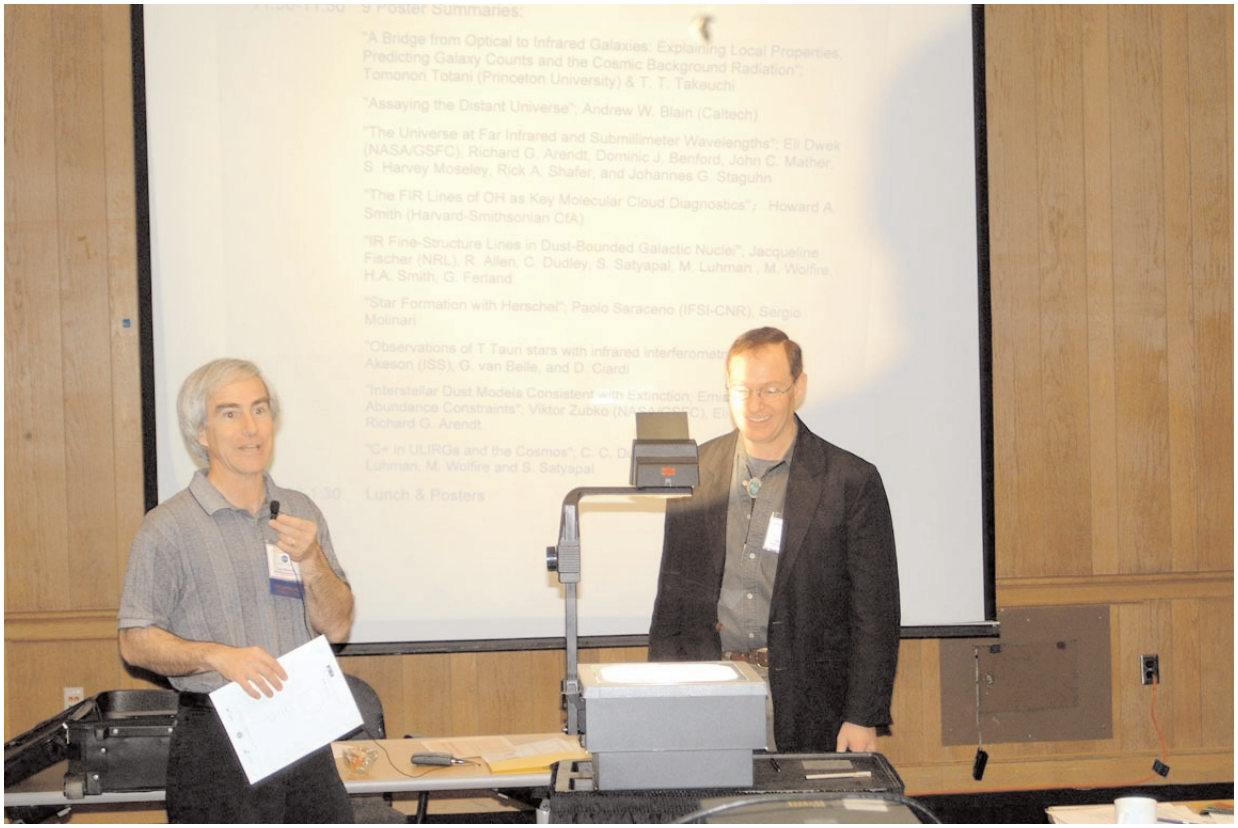
Poster Summaries:
"A Bridge from Optical to Infrared Galaxies: Explaining Local Properties, Predicting Galaxy Counts and the Cosmic Background Radiation"; Tomonori Totani (Princeton University) & T. T. Takeuchi
"Assaying the Distant Universe"; Andrew W. Blain (Caltech)
"The Universe at Far Infrared and Submillimeter Wavelengths"; Eli Dwek (NASA/GSFC), Richard G. Arendt, Dominic J. Benford, John C. Mather, S. Harvey Moseley, Rick A. Shafer, and Johannes G. Staguhn
"The FIR Lines of OH as Key Molecular Cloud Diagnostics"; Howard A. Smith (Harvard-Smithsonian CfA)
"IR Fine-Structure Lines in Dust-Bounded Galactic Nuclei"; Jacqueline Fischer (NRL), R. Allen, C. Dudley, S. Satyapal, M. Luhman , M. Wolfire, H.A. Smith, G. Ferland
"Star Formation with Herschel"; Paolo Saraceno (IFSI-CNR), Sergio Molinari
"Observations of T Tauri stars with infrared interferometry"; Axeson (ISS), G. van Belle, and D. Ciardi
"Interstellar Dust Models Consistent with Extinction, Emi... Abundance Constraints"; Viktor Zubko [NA... Richard G. Arendt
"C+ in ULIRGs and the Cosmos"; C. C. D... Luhman, M. Wolfire and S. Satyapal
Lunch & Posters